

# FERMI OBSERVATION OF THE TRANSITIONAL PULSAR BINARY XSS J12270–4859

YI XING AND ZHONGXIANG WANG

Key Laboratory for Research in Galaxies and Cosmology, Shanghai Astronomical Observatory,  
 Chinese Academy of Sciences, 80 Nandan Road, Shanghai 200030, China

*Draft version November 14, 2014*

## ABSTRACT

Because of the disappearance of its accretion disk since the time period around 2012 November–December, XSS J12270–4859 has recently been identified as, in addition to PSR J1023+0038, another transitional millisecond pulsar binary. We have carried out detailed analysis of the *Fermi* Large Area Telescope data for the binary. While both spectra before and after the disk-disappearance transition are well described by an exponentially cut-off power law, typical for pulsars’ emission in the *Fermi*’s 0.2–300 GeV, a factor of 2 flux decrease related to the transition is detected. A weak orbital modulation is seen, but only detectable in the after-transition data, same to that found at X-rays. In the long-term light curve of the source before the transition, a factor of 3 flux variations are seen. Comparing to the properties of J1023+0038, we discuss the implications from these results. We suggest that since the modulation is aligned with that at X-rays in orbital phase, it possibly arises due to the occultation of the  $\gamma$ -ray emitting region by the companion. The origin of the variations in the long-term light curve is not clear, because the source field also contains unidentified radio or X-ray sources and their contamination can not be excluded. Multi-wavelength observations of the source field will help identify the origin of the variations by detecting any related flux changes from the in-field sources.

*Subject headings:* binaries: close — stars: individual (XSS J12270–4859) — stars: low-mass — stars: neutron

## 1. INTRODUCTION

It is clear now that during the evolution from low-mass X-ray binaries (LMXBs) to millisecond pulsars (MSPs; e.g., Bhattacharya & van den Heuvel 1991), a neutron star in such a system can switch between the states of being accretion-powered and rotation-powered, which is well illustrated from observational studies of the MSP binary J1824–2452I in the globular cluster M28 (Papitto et al. 2013). Before, indirect evidence has strongly suggested that several accreting MSPs in transient LMXBs probably switch to be rotation powered during their quiescent states (Burderi et al. 2003; Wang et al. 2013 and references therein). The discovery of the radio MSP binary J1023+0038 (Archibald et al. 2009) has further shown interesting features for probably the end phase of the evolution: such a binary can switch between the states of having an accretion disk and being disk-free, while the pulsar in the binary is still active but not observable during the former state (Stappers et al. 2014; Coti Zelati et al. 2014). PSR J1023+0038 is also a prototypical, so-called ‘redback’ system (Roberts 2013). Different from those ‘black widow’ MSP binaries (e.g., B1957+20; Fruchter et al. 1988) that contain very low-mass ( $\sim 0.02 M_{\odot}$ ) companions, redback systems have relatively massive secondaries ( $\sim 0.1$ – $0.6 M_{\odot}$ ). Irradiation and/or evaporation of the companion by emission and pulsar wind, respectively, from the central neutron star probably play an important role in forming black widow and redback systems (Chen et al. 2013; Benvenuto et al. 2014).

The second transitional MSP binary, XSS J12270–4859, was recently identified, as the accretion disk in the system was found to have disappeared since 2012 Nov.–Dec. (Bassa et al. 2014; de Martino et al. 2014). Discovered by the Rossi X-ray Timing Explorer

(Sazonov & Revnivtsev 2004) and initially thought as a cataclysmic variable (Masetti et al. 2006), the binary was considered as a peculiar LMXB that is associated with the  $\gamma$ -ray source 2FGL J1227.7–4853 (Hill et al. 2011; de Martino et al. 2013 and references therein). After its transition to be disk-free, multiple energy observations have revealed its full nature. The detection of a 1.69 ms radio pulsar was reported (Roy et al. 2014; Ray et al. 2014). Optical observations have found that its orbital period is 6.9 hr (Bassa et al. 2014; de Martino et al. 2014), and the companion is a mid G-type, under-massive donor star with mass of  $0.06$ – $0.12 M_{\odot}$  (de Martino et al. 2014), establishing it as another redback system. At X-ray energies, the binary is an order of magnitude fainter than before, with orbital modulation present (Bogdanov et al. 2014). Comparing to that seen in J1023+0038 in the disk-free state (Archibald et al. 2010; Bogdanov et al. 2011), the X-ray emission likely has an intrabinary-shock origin (Bogdanov et al. 2014), due to the interaction between the outflow from the companion and the pulsar wind. At  $\gamma$ -ray energies, a possible flux decrease was also reported in an astronomer’s telegram (Tam et al. 2013). These properties are highly comparable to that of J1023+0038, particularly since the latter system just underwent a transition to the active accretion state in 2013 June and extensive observational studies have been conducted (Stappers et al. 2014; Patruno et al. 2014; Takata et al. 2014; Coti Zelati et al. 2014).

The source field of 2FGL J1227.7–4853 was found to contain three radio sources (Hill et al. 2011). The brightest one J122806–485218 has extended radio emission, although its radio properties likely do not support the classification of it being a blazar (Hill et al. 2011), the class for which is the major population

( $\sim 80\%$ ) detected by *Fermi* in its Large Area Telescope (LAT) second source catalog (Nolan et al. 2012). X-ray observations did not reveal any physical connection between XSS J12270–4859 and J122806–485216, but found a possible, previously uncatalogued galaxy cluster that is located approximately  $1'$  away from the former (Bogdanov et al. 2014). Previously, Hill et al. (2011) and de Martino et al. (2013) have analyzed approximately 2-yr and 4-yr *Fermi* data for 2FGL J1227.7–4853, respectively, and mainly studied its  $\gamma$ -ray spectral properties.

Given above and the recent identification of the transitional MSP binary nature for XSS J12270–4859, detailed analysis of the *Fermi* data is needed, which possibly helps our understanding of the physical processes in this system. We have carried out the analysis to identify the properties of the associated  $\gamma$ -ray source, study its long-term flux variability, and search for modulation signals. In this paper, we report the results from the analysis. We describe the *Fermi* observation data in § 2, and present the data analysis and results in § 3. Discussion of the results is given in § 4.

## 2. OBSERVATION

LAT is a  $\gamma$ -ray imaging instrument onboard *Fermi*. It makes all-sky survey in an energy range from 20 MeV to 300 GeV (Atwood et al. 2009). In our analysis, we selected LAT events from the *Fermi* Pass 7 Reprocessed (P7REP) database inside a  $20^\circ \times 20^\circ$  region centered at the position of XSS J12270–4859, which is R.A.=186°99'47.83, Decl.=−48°89'52.44 (equinox J2000.0) obtained from the Two Micron All Sky Survey (2MASS, Cutri et al. 2003) and used in Bogdanov et al. (2014) for X-ray studies of orbital modulation of this source. We kept events during the time period from 2008-08-04 15:43:36 (UTC) to 2014-07-10 18:16:37 (UTC) and in the energy range of 100 MeV to 300 GeV. In addition, only events with zenith angle less than 100 deg and during good time intervals were selected. The former prevents the Earth's limb contamination, and for the latter, the quality of the data was not affected by the spacecraft events.

## 3. DATA ANALYSIS AND RESULTS

### 3.1. Source Identification

We included all sources within 16 deg in the *Fermi* second source catalog (Nolan et al. 2012) centered at the position of XSS J12270–4859 to make the source model. The spectral function forms of the sources are provided in the catalog. The spectral normalization parameters of the sources within 8 deg from XSS J12270–4859 were set free, and all other parameters of the sources were fixed at their catalog values. We used the spectrum model `gll_iem_v05_rev1.fits` and the spectrum file `iso_source_v05.txt` for the Galactic and the extragalactic diffuse emission, respectively, in the source model. The normalizations of the diffuse components were set as free parameters.

Using the LAT science tools software package `v9r33p0`, we performed standard binned likelihood analysis to the LAT data in the  $>0.2$  GeV range. Events below 200 MeV were rejected because of the relative large uncertainties of the instrument response function of the LAT

in the low energy range. We extracted the Test Statistic (TS) map of a  $2^\circ \times 2^\circ$  region centered at the position of XSS J12270–4859 (Figure 1), with all sources in the source model considered except the candidate  $\gamma$ -ray counterpart (2FGL J1227.7–4853) to XSS J12270–4859. The TS value at a specific position, calculated from  $TS = -2 \log(L_0/L_1)$  (where  $L_0$  and  $L_1$  are the maximum likelihood values for a model without and with an additional source respectively), is a measurement of the fit improvement for including the source, and is approximately the square of the detection significance of the source (Abdo et al. 2010).

As shown in Figure 1, the  $\gamma$ -ray emission near the center was detected with  $TS \simeq 1440$ , indicating  $\sim 37\sigma$  detection significance. We ran `gtfindsrc` in the LAT software package to find the position of the  $\gamma$ -ray source and obtained R.A.=186°99, Decl.=−48°90 (equinox J2000.0), with  $1\sigma$  nominal uncertainty of  $0^\circ 03$ . This best-fit position is consistent with the 2MASS position of XSS J12270–4859 (mark by a dark cross in Figure 1). The offset between the two positions is only  $\sim 0^\circ 01$ . The nearby radio source J122806–485218 and possible galaxy cluster J122807.4–48532 are also within the  $2\sigma$  error circle, which are  $\simeq 0^\circ 04$  and  $\simeq 0^\circ 03$  away from the best-fit position, respectively.

Including the  $\gamma$ -ray source in the source model at the 2MASS position of XSS J12270–4859, we performed standard binned likelihood analysis to the LAT data in  $>0.2$  GeV range, with emission of this source modeled with a simple power law and an exponentially cutoff power law (characteristic of pulsars). For the former model, photon index  $\Gamma = 2.41 \pm 0.03$  with a  $TS_{pl}$  value of  $\sim 1446$  was obtained, and for the latter,  $\Gamma = 2.11 \pm 0.08$  and cutoff energy  $E_c = 6 \pm 2$  GeV, with a  $TS_{exp}$  value of  $\sim 1466$ , were obtained. These results are also given in Table 1. The low-energy cutoff was thus detected with  $>4\sigma$  significance (estimated from  $\sqrt{TS_{cutoff}}$ , where  $TS_{cutoff} \simeq TS_{exp} - TS_{pl} \simeq 20$ ). The result favors the association of the  $\gamma$ -ray source with the pulsar binary system XSS J12270–4859.

### 3.2. Variability Analysis

We obtained the light curve of the source in  $>0.2$  GeV energy range to search for flux variations, particularly around the state-transition time period of XSS J12270–4859. A point source with  $\Gamma = 2.41$  power-law emission (§ 3.1) at the 2MASS position was considered. Significant variations before the state change (MJD 56245) are seen in the 30-day time interval light curve. In Figure 2, the light curve as well as the TS curve are shown. The flux has a factor of 3 variations ( $2\text{--}6 \times 10^{-8}$  photons  $\text{cm}^{-2} \text{ s}^{-1}$ ), while TS varies between 10–70. After the state change (around MJD 56283),  $\gamma$ -ray emission was relatively stable, with the flux and TS being  $\sim 2 \times 10^{-8}$  photons  $\text{cm}^{-2} \text{ s}^{-1}$  and  $\sim 20$  for most of the time. We noted that there were two unreliable data points at the time bins of MJD 56573–56603 and 56663–56693. The obtained TS values are smaller than 1 (marked by open symbols in Figure 2). During the times, there were two target-of-opportunity observations causing data gaps of  $\sim 5$  and  $\sim 12$  days, respectively.

To further investigate the flux variations during the transition time period, we constructed a 30-day light

curve by shifting each time interval by 1 day forward and obtaining the flux during such a 30-day interval (see, e.g., Takata et al. 2014). The resulting fine smooth light curve is shown in the inset box of Figure 2. A factor of 2 flux decrease, from  $\sim 4 \times 10^{-8}$  to  $\sim 2 \times 10^{-8}$  photons  $\text{cm}^{-2} \text{s}^{-1}$ , is clearly visible. Therefore 2FGL J1227.7–4853 had a flux change related to the state transition.

We performed standard binned likelihood analysis to the LAT data in  $>0.2$  GeV range for the time periods before and after the state change. When a power-law spectrum was assumed for the former data, we found  $\Gamma = 2.42 \pm 0.04$  with  $\text{TS}_{pl} \simeq 1247$  and for the latter,  $\Gamma = 2.42 \pm 0.09$  with a  $\text{TS}_{pl} \simeq 183$ . When an exponentially cutoff power law was considered, the respective results were  $\Gamma = 2.13 \pm 0.08$  and  $E_c = 6 \pm 2$  GeV with  $\text{TS}_{exp} \simeq 1262$ , and  $\Gamma = 1.8 \pm 0.3$  and  $E_c = 2 \pm 1$  GeV with  $\text{TS}_{exp} \simeq 192$ . Therefore the low-energy cutoff was detected with  $\text{TS}_{cutoff}$  values of  $\simeq 15$  and  $\simeq 9$ , which correspond to the detection significance of  $\simeq 3.8\sigma$  and  $\simeq 3\sigma$  before and after the state change, respectively. These results indicate that the  $\gamma$ -ray emission from the source is likely better described by a spectrum characteristic of pulsars, and the emission after the state transition is harder. For the exponentially cutoff power-law spectra, the  $>0.2$  GeV  $\gamma$ -ray fluxes were  $3.2 \pm 0.2 \times 10^{-8}$  and  $1.7 \pm 0.2 \times 10^{-8}$  photons  $\text{cm}^{-2} \text{s}^{-1}$  during the time periods before and after the state change, respectively. These results are summarized in Table 1.

### 3.3. Spectral Analysis

We report our spectrum results of the  $\gamma$ -ray source by considering the emission as a point source with a power-law spectrum at the 2MASS position. The photon index was fixed to the value we obtained above using the total data (see Table 1). The spectrum was extracted by performing maximum likelihood analysis to the LAT data in 10 evenly divided energy bands in logarithm from 0.1–300 GeV. Only spectral points with  $\text{TS} \geq 4$  were kept. We extracted  $\gamma$ -ray spectra for the time periods before and after the state change, respectively. The obtained spectra are shown in the left panel of Figure 3, and the energy flux values are given in Table 2.

In order to investigate the variability before the state transition, we also extracted  $\gamma$ -ray spectra from the data in the time intervals of  $\text{TS} \geq 35$  (‘high’ state) and  $\text{TS} \leq 20$  (‘low’ state). The obtained spectra are shown in the right panel of Figure 3, with the energy flux values given in Table 2. Comparing the two spectra, while the source appeared brighter across the whole energy range in the high state, the flux at 0.33 GeV, showing a  $\simeq 5\sigma$  difference, had the most significant change.

### 3.4. Timing Analysis

We performed timing analysis to the LAT data of XSS J12270–4859 to search for possible orbital modulations. Considering the X-ray orbital modulation was only detected after the state change (Bogdanov et al. 2014), we first folded the LAT data of the  $\gamma$ -ray source during the time period at the optical orbital frequency of  $4.01850 \pm 0.00003 \times 10^{-5}$  Hz (de Martino et al. 2014; see also Bassa et al. 2014). The 2MASS position of XSS J12270–4859 was used for the barycentric corrections to

photon arrival times, and photons within  $1^\circ.2$  from the position were collected. Different energy ranges (e.g.,  $>0.2$ ,  $>0.3$ ,  $>0.5$ ,  $>1$ , and  $>2$  GeV) were tested in folding. We found that the highest orbital signal was revealed in the  $>0.3$  GeV energy range. The folded light curve, which has an H-test value of  $\sim 10$  (corresponding to  $3\sigma$  detection significance), is shown in Figure 4. The phase zero is set at the ascending node of the pulsar in XSS J12270–4859. Although the significance is not high, we note that the folded light curve is nearly aligned with the X-ray one given in Bogdanov et al. (2014), which strengthens the modulation detection. The result thus provides strong evidence for the association of the  $\gamma$ -ray source with XSS J12270–4859.

As a test, we also folded the LAT data of XSS J12270–4859 before the state change at the optical orbital frequency. No significant  $\gamma$ -ray modulation was detected (the H-test values were  $\sim 0.3$ ).

We made two  $>0.3$  GeV TS maps over the phase ranges of 0.1–0.4 (named Phase I) and 0.6–0.9 (named Phase II), which approximately are the bottom and peak, respectively, of the orbital modulation (Figure 4). The obtained TS maps are shown in Figure 5. The source during Phase II is more significantly detected than during Phase I, as the TS values are  $\simeq 76$  and  $\simeq 20$ , respectively. We also ran *gtfindsrc* to determine the positions of the  $\gamma$ -ray emission during the two phases, and found that they are consistent with the position of XSS J12270–4859 within  $2\sigma$  error circles. The analysis confirms the detection of orbital modulation from the photon folding.

Spectra during Phase I and Phase II were also obtained, but due to limited numbers of photons, the uncertainties on the flux data points are too large to allow any further detailed analysis.

## 4. DISCUSSION

From our analysis of the *Fermi* data of 2FGL J1227.7–4853, we have detected a flux decrease during the state transition of XSS J12270–4859, which occurred around 2012 Nov.–Dec.. We have also detected orbital modulation, although weakly, only in the data after the transition, consistent with the result from the X-ray observation (Bogdanov et al. 2014). Both detections are strong evidence for the association between the two sources. In addition, the exponentially cutoff power-law model, which is a typical spectrum for pulsar emission at the *Fermi* LAT  $\gamma$ -ray energy range (Abdo et al. 2013), is preferred to describe the source’s emission during both before and after the transition time periods. This result supports the association as well. Given these, our analysis has confirmed the previous identification that 2FGL J1227.7–4853 is the  $\gamma$ -ray counterpart to XSS J12270–4859 (Hill et al. 2011; de Martino et al. 2013).

From extensive observations, particularly at  $\gamma$ -ray band, of the state transition of PSR J1023+0038 that occurred in 2013 June, it has been learned that in the state of having an accretion disk,  $\gamma$ -ray emission is brighter than that in the disk-free state: there was an order of magnitude flux increase in J1023+0038 accompanying the state transition (Stappers et al. 2014; Takata et al. 2014). What we have detected in XSS J12270–4859 is the opposite to that of the J1023+0038 case in 2013, while the flux change is smaller, as the flux in the latter state is approximately two-times lower

than that in the former. It is very likely that  $\gamma$ -ray emission in the disk-free state originates from the magnetosphere of the pulsar, while the brighter emission in the accretion state has been proposed to be due to inverse Compton (IC) scattering of a cold pulsar wind off the optical/infrared photons from the accretion disk (Takata et al. 2014) or self-synchrotron Compton processes at the magnetospheric region of a propelling neutron star (Papitto et al. 2014). Similar to that in J1023+0038,  $\Gamma = 1.8 \pm 0.2$  and  $E_c = 2.3 \pm 0.9$  GeV to  $1.4 \pm 0.6$  and  $0.7 \pm 0.4$  GeV from the accretion state to disk-free state, spectral changes were also detected in XSS J12270–4859, as  $\Gamma \simeq 2.13$  and  $E_c \simeq 6$  GeV in the former changed to  $\simeq 1.8$  and  $\simeq 2$  GeV in the latter. Although the large uncertainties do not allow us to draw a clear conclusion, the measurements are possible evidence for that the exact same physical processes occurred in XSS J12270–4859.

Probably because J12270–4859 is approximately 3 times brighter than J1023+0038 in the disk-free state (Tam et al. 2010), we have likely detected its orbital modulation. Such  $\gamma$ -ray modulation, which was seen marginally in the black widow binary PSR B1957+20 (and the candidate MSP binary 2FGL J0523.3–2530; Wu et al. 2012; Xing et al. 2014), has been suggested to arise due to the view angle of the intrabinary interaction region (Wu et al. 2012; Bednarek 2014). However the modulation, approximately aligned with that at X-rays (Bogdanov et al. 2014), has the brightness peak in the orbital phase of 0.5–1.0 (around the superior conjunction when the companion is behind the neutron star). This orbital variation is different from that in B1957+20, as its brightness peak is at the opposite phase region. In the latter case the inverse Compton processes, which produces extra  $\gamma$ -ray emission around the inferior conjunction phase, has been suggested to be viewed as a head-on collision between the pulsar wind and the soft photons from the pulsar or the companion (Wu et al. 2012; Bednarek 2014). For XSS J12270–4859, we suspect its modulation may arise because of the occultation of the photon emitting region by the companion, which well explains the X-ray modulation in PSR J1023+0038 (see Bogdanov et al. 2011 for details). We note that the

inclination angle of the binary was estimated to be  $45^\circ$ – $65^\circ$  (de Martino et al. 2014), also similar to that of PSR J1023+0038 (Wang et al. 2009). Unfortunately, the photon counts were too low to allow a comparison of the phase-resolved spectra (obtained in the bright and faint phase ranges), which might help identify the cause of the modulation. If it were due to the occultation, no spectral changes would be expected.

In addition to the flux change related to the state transition, our data analysis shows that  $\gamma$ -ray emission from XSS J12270–4859 may not be stable before the state change, possibly having a factor of 3 flux variations in its long-term light curve. The spectrum comparison between the high (with TS greater than 35) and low (with TS lower than 20) states only indicates the possible presence of an extra component around 0.33 GeV; otherwise similar flux changes were across the whole energy range. Such flux variations are not seen before in MSP binaries. Recently in the candidate MSP binary 2FGL J0523.3–2530, significant flux variations were detected but that was caused by the presence of a 2–3 GeV component in the high state (Xing et al. 2014). Given that there are three radio sources and a possible galaxy cluster in the source field, contamination from them can not be totally excluded. If one of them is associated with an unidentified blazer, which would have caused the flux changes across the *Fermi* energy range due to its variability (e.g., Williamson et al. 2014), the flux variations would instead indicate the contamination. In order to determine this possibility by detecting any related flux changes at radio or X-ray energies, multi-wavelength observations can be carried out when 2FGL J1227.7–4853 shows significant brightening again.

This research was supported by supported by Shanghai Natural Science Foundation for Youth (13ZR1464400), the National Natural Science Foundation of China (11373055), and the Strategic Priority Research Program “The Emergence of Cosmological Structures” of the Chinese Academy of Sciences (Grant No. XDB090000000). Z.W. is a Research Fellow of the One-Hundred-Talents project of Chinese Academy of Sciences.

## REFERENCES

- Abdo, A. A., Ackermann, M., Ajello, M., et al. 2010, *ApJS*, 188, 405
- Abdo, A. A., Ajello, M., Allafort, A., et al. 2013, *ApJS*, 208, 17
- Archibald, A. M., Kaspi, V. M., Bogdanov, S., et al. 2010, *ApJ*, 722, 88
- Archibald, A. M., Stairs, I. H., Ransom, S. M., et al. 2009, *Science*, 324, 1411
- Atwood, W. B., Abdo, A. A., Ackermann, M., et al. 2009, *ApJ*, 697, 1071
- Bassa, C. G., Patruno, A., Hessels, J. W. T., et al. 2014, *MNRAS*, 441, 1825
- Bednarek, W. 2014, *A&A*, 561, A116
- Benvenuto, O. G., De Vito, M. A., & Horvath, J. E. 2014, *ApJ*, 786, L7
- Bhattacharya, D., & van den Heuvel, E. P. J. 1991, *Phys. Rep.*, 203, 1
- Bogdanov, S., Archibald, A. M., Hessels, J. W. T., et al. 2011, *ApJ*, 742, 97
- Bogdanov, S., Patruno, A., Archibald, A. M., et al. 2014, *ApJ*, 789, 40
- Burderi, L., Di Salvo, T., D’Antona, F., et al. 2003, *Chinese Journal of Astronomy and Astrophysics Supplement*, 3, 311
- Chen, H.-L., Chen, X., Tauris, T. M., & Han, Z. 2013, *ApJ*, 775, 27
- Coti Zelati, F., Baglio, M. C., Campana, S., et al. 2014, *MNRAS*, 444, 1783
- Cutri, R. M., Skrutskie, M. F., van Dyk, S., et al. 2003, *VizieR Online Data Catalog*, 2246, 0
- de Martino, D., Belloni, T., Falanga, M., et al. 2013, *A&A*, 550, A89
- de Martino, D., Casares, J., Mason, E., et al. 2014, *ArXiv e-prints*
- Fruchter, A. S., Stinebring, D. R., & Taylor, J. H. 1988, *Nature*, 333, 237
- Hill, A. B., Szostek, A., Corbel, S., et al. 2011, *MNRAS*, 415, 235
- Masetti, N., Morelli, L., Palazzi, E., et al. 2006, *A&A*, 459, 21
- Nolan, P. L., Abdo, A. A., Ackermann, M., et al. 2012, *ApJS*, 199, 31
- Papitto, A., Torres, D. F., & Li, J. 2014, *MNRAS*, 438, 2105
- Papitto, A., Ferrigno, C., Bozzo, E., et al. 2013, *Nature*, 501, 517
- Patruno, A., Archibald, A. M., Hessels, J. W. T., et al. 2014, *ApJ*, 781, L3
- Ray, P. S., Roy, J., Bhattacharyya, B., Deneva, J. S., & Camilo, F. M. 2014, in *AAS/High Energy Astrophysics Division*, Vol. 14, *AAS/High Energy Astrophysics Division*, 122.26

- Roberts, M. S. E. 2013, in IAU Symposium, Vol. 291, IAU Symposium, ed. J. van Leeuwen, 127–132
- Roy, J., Bhattacharyya, B., & Ray, P. S. 2014, *The Astronomer's Telegram*, 5890, 1
- Sazonov, S. Y., & Revnivtsev, M. G. 2004, *A&A*, 423, 469
- Stappers, B. W., Archibald, A. M., Hessels, J. W. T., et al. 2014, *ApJ*, 790, 39
- Takata, J., Li, K. L., Leung, G. C. K., et al. 2014, *ApJ*, 785, 131
- Tam, P. H. T., Kong, A. K. H., & Li, K. L. 2013, *The Astronomer's Telegram*, 5652, 1
- Tam, P. H. T., Hui, C. Y., Huang, R. H. H., et al. 2010, *ApJ*, 724, L207
- Wang, Z., Archibald, A. M., Thorstensen, J. R., et al. 2009, *ApJ*, 703, 2017
- Wang, Z., Breton, R. P., Heinke, C. O., Deloye, C. J., & Zhong, J. 2013, *ApJ*, 765, 151
- Williamson, K. E., Jorstad, S. G., Marscher, A. P., et al. 2014, *ApJ*, 789, 135
- Wu, E. M. H., Takata, J., Cheng, K. S., et al. 2012, *ApJ*, 761, 181
- Xing, Y., Wang, Z., & Ng, C.-Y. 2014, *ArXiv e-prints*

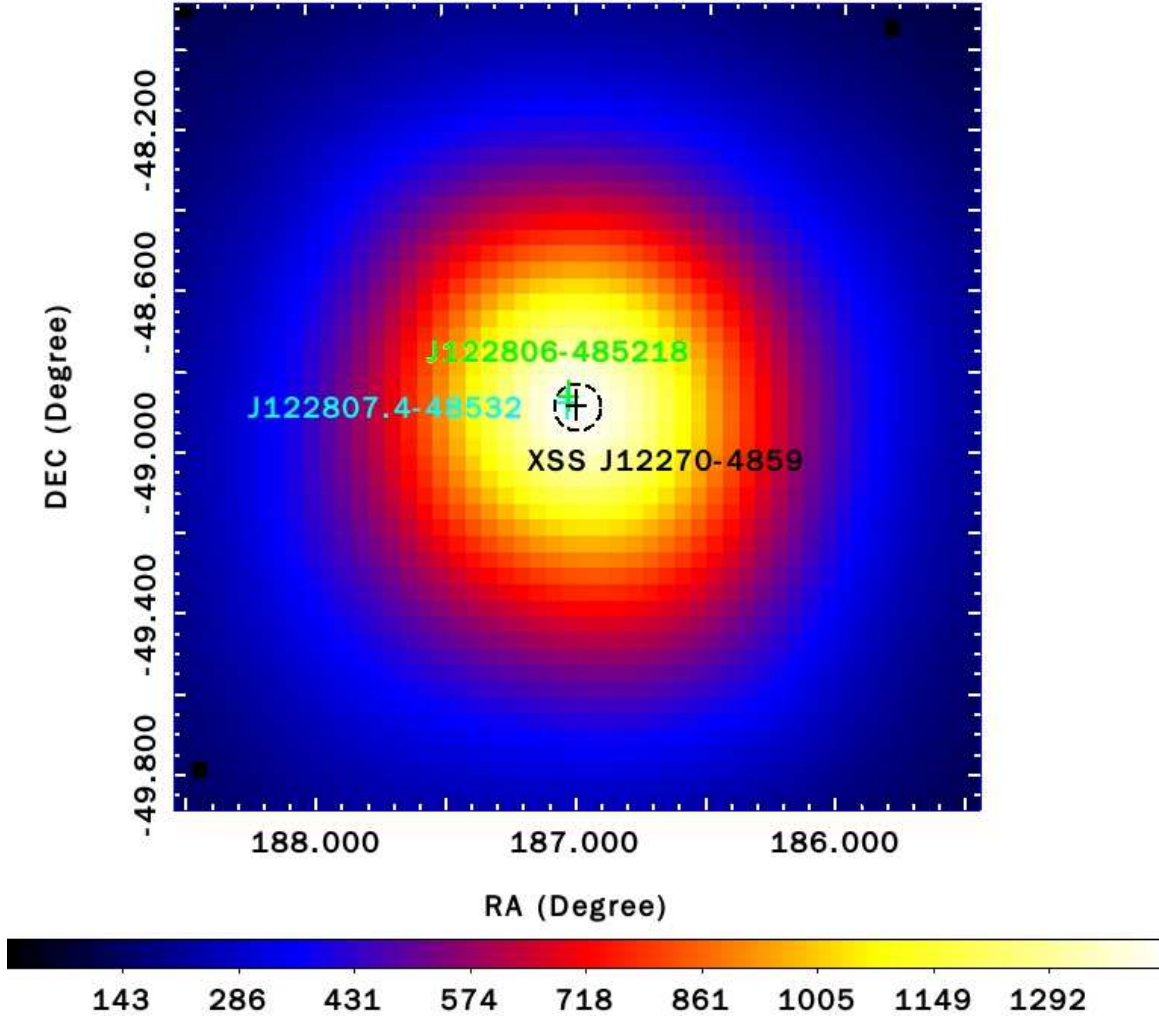


FIG. 1.— 200 MeV–300 GeV TS map of a  $2^\circ \times 2^\circ$  region centered at the position of XSS J12270–4859. The image scale of the map is  $0.04^\circ \text{ pixel}^{-1}$ . All sources in the source model were considered and removed. The dark cross, green cross, light blue cross, and the dashed black circle mark the 2MASS position of XSS J12270–4859, the nearby brightest radio source, the nearby galaxy cluster, and the  $2\sigma$  error circle of the best-fit position obtained from using the *Fermi* data, respectively.

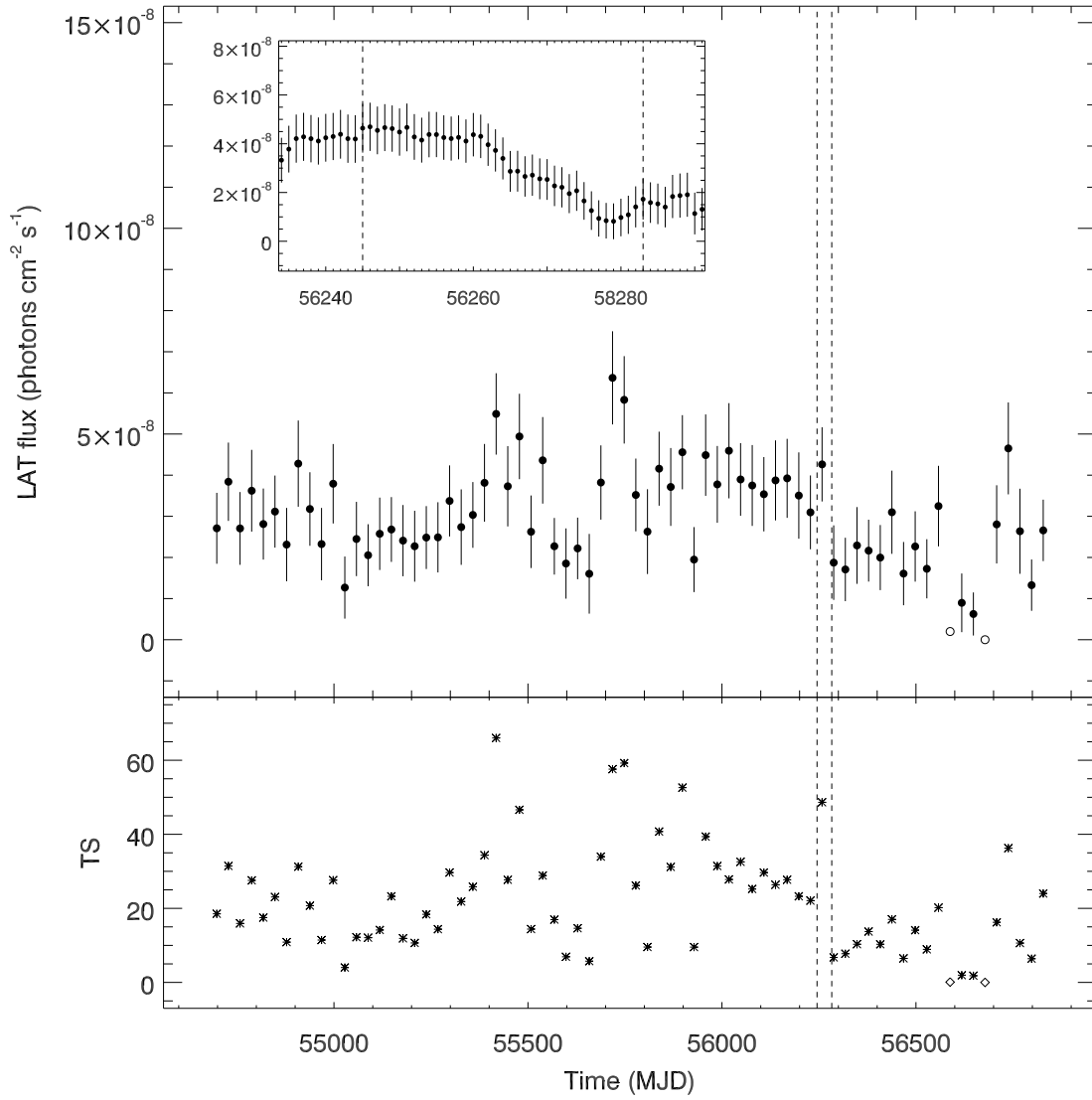


FIG. 2.— 30-day interval light curve and TS curve of 2FGL J1227.7–4853. The dashed lines mark the time period of the state transition, and the inset panel shows the detailed flux changes during the time period.

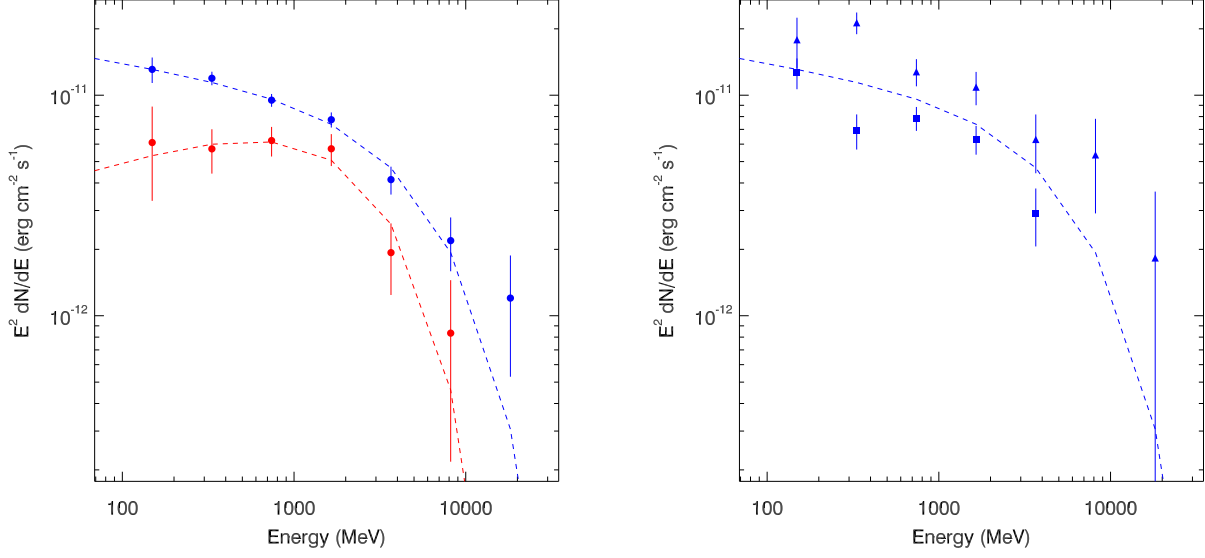


FIG. 3.— *Left panel:*  $\gamma$ -ray spectra of 2FGL J1227.7–4853 obtained before (blue data points) and after (red data points) the state transition. *Right panel:*  $\gamma$ -ray spectra of 2FGL J1227.7–4853 obtained during the high (triangle data points) and low (square data points) states. The exponentially cutoff power laws obtained from maximum likelihood analysis before and after the state transition are shown as blue and red dashed curves.



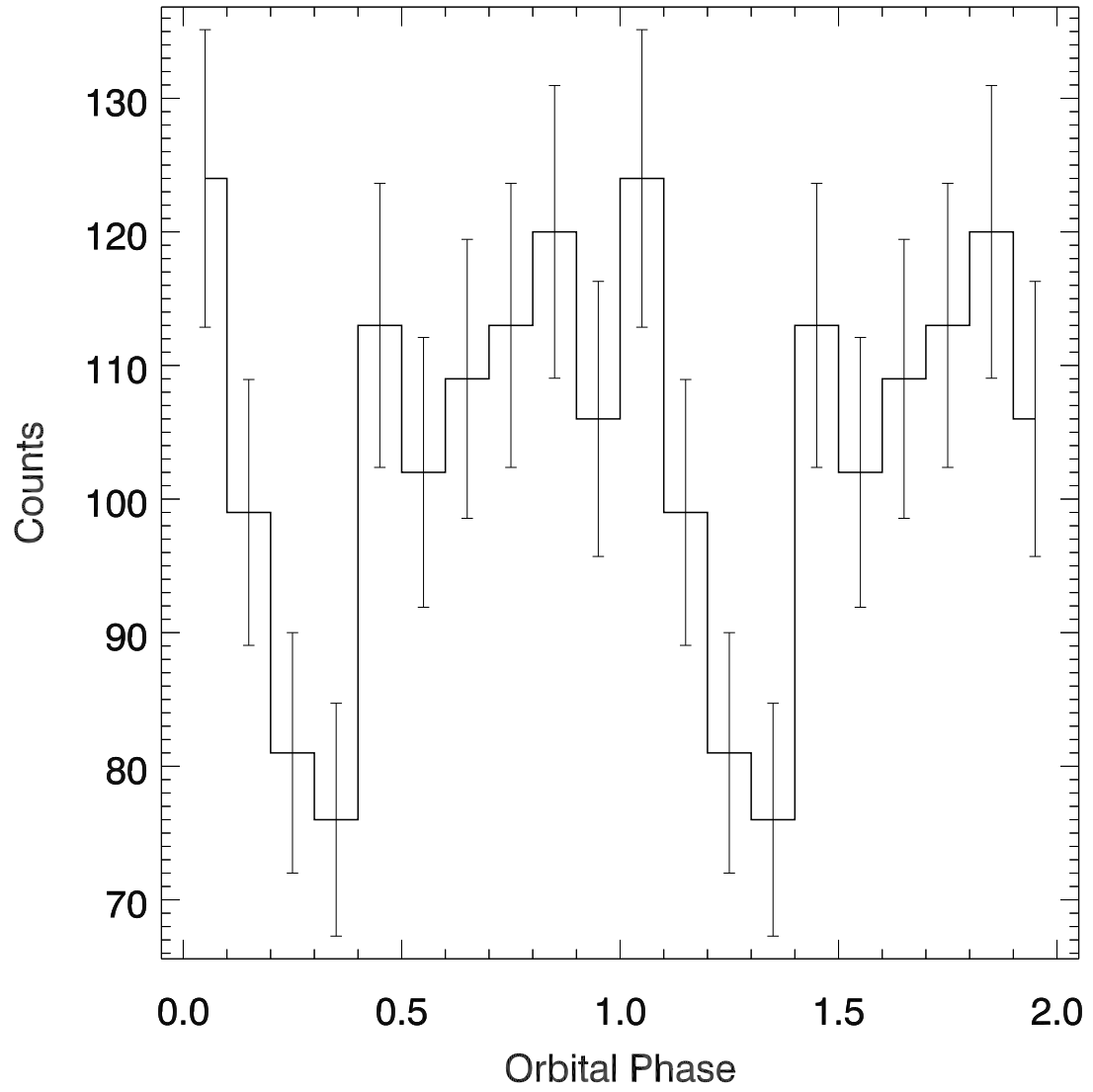


FIG. 4.— 0.3–300 GeV light curve folded at the optical orbital period, obtained from the data after the state transition.

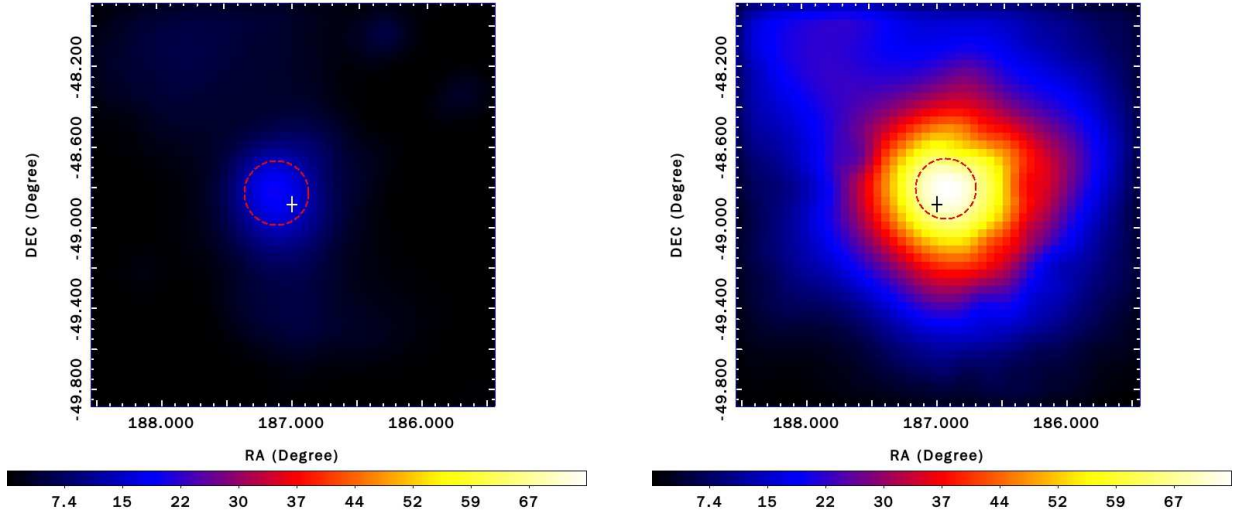


FIG. 5.— 0.3–300 GeV TS maps of a  $2^\circ \times 2^\circ$  region centered at the position of XSS J12270–4859 for Phase I (*left panel*) and Phase II (*right panel*). The image scale of the maps is  $0.04^\circ \text{ pixel}^{-1}$ . The white (*left panel*) and dark (*right panel*) crosses mark the 2MASS position of XSS J12270–4859, and the dashed red circles indicate the  $2\sigma$  error circles of the best-fit positions of 2FGL J1227.7–4853 during the two phases.

TABLE 1  
 BINNED LIKELIHOOD ANALYSIS RESULTS FOR 2FGL J1227.7–4853.

	Spectral model	Flux/ $10^{-9}$ (photon $\text{cm}^{-2} \text{s}^{-1}$ )	$\Gamma$	$E_c$ (GeV)	TS
Total data	Power law	$30 \pm 1$	$2.41 \pm 0.03$	$\dots$	1446
	Power law with cutoff	$28 \pm 1$	$2.11 \pm 0.08$	$6 \pm 2$	1466
Before state change	Power law	$33 \pm 1$	$2.42 \pm 0.04$	$\dots$	1247
	Power law with cutoff	$32 \pm 2$	$2.13 \pm 0.08$	$6 \pm 2$	1262
After state change	Power law	$20 \pm 2$	$2.42 \pm 0.09$	$\dots$	183
	Power law with cutoff	$17 \pm 2$	$1.8 \pm 0.3$	$2 \pm 1$	192

TABLE 2  
FLUX MEASUREMENTS OF 2FGL J1227.7–4853.

E (GeV)	$F_{\text{low}}/10^{-12}$ (erg cm $^{-2}$ s $^{-1}$ )	$F_{\text{high}}/10^{-12}$ (erg cm $^{-2}$ s $^{-1}$ )	$F_{\text{before}}/10^{-12}$ (erg cm $^{-2}$ s $^{-1}$ )	$F_{\text{after}}/10^{-12}$ (erg cm $^{-2}$ s $^{-1}$ )
0.15	$13 \pm 2$	$18 \pm 5$	$13 \pm 2$	$6 \pm 3$
0.33	$7 \pm 1$	$21 \pm 2$	$11.9 \pm 0.8$	$6 \pm 1$
0.74	$8 \pm 1$	$13 \pm 2$	$9.5 \pm 0.6$	$6 \pm 1$
1.65	$6.3 \pm 0.9$	$11 \pm 2$	$7.7 \pm 0.6$	$5.7 \pm 0.9$
3.67	$2.9 \pm 0.9$	$6 \pm 2$	$4.1 \pm 0.6$	$1.9 \pm 0.7$
8.17	...	$5 \pm 2$	$2.2 \pm 0.6$	$0.8 \pm 0.6$
18.20	...	$2 \pm 2$	$1.2 \pm 0.7$	...

NOTE. — Columns 2 and 3 list the energy flux ( $E^2 \times \text{dN/dE}$ ) in each energy bin during the low and high states before the state change, respectively. Column 4 and 5 list the energy flux ( $E^2 \times \text{dN/dE}$ ) in each energy bin during the observations before and after the state change, respectively.